THE JOURNAL OF BIOLOGICAL CHEMISTRY VOL. 290, NO. 52, pp. 30771–30782, December 25, 2015

Regulation of Focal Adhesion Dynamics and Cell Motility by the EB2 and Hax1 Protein Complex*[S]

Received for publication, June 11, 2015, and in revised form, October 30, 2015 Published, JBC Papers in Press, November 2, 2015, DOI 10.1074/jbc.M115.671743

Han Liu[‡], Jiping Yue[‡], He Huang[‡], Xuewen Gou[‡], Shao-Yu Chen[§], Yingming Zhao[‡], and Xiaoyang Wu[‡1]

From the [‡]Ben May Department for Cancer Research, University of Chicago, Chicago, Illinois 60637 and the [§]Department of Pharmacology and Toxicology, University of Louisville Health Science Center, Louisville, Kentucky, 40292

Cell migration is a fundamental cellular process requiring integrated activities of the cytoskeleton, membrane, and cell/extracellular matrix adhesions. Many cytoskeletal activities rely on microtubule filaments. It has been speculated that microtubules can serve as tracks to deliver proteins essential for focal adhesion turnover. Three microtubule end-binding proteins (EB1, EB2, and EB3) in mammalian cells can track the plus ends of growing microtubules. EB1 and EB3 together can regulate microtubule dynamics by promoting microtubule growth and suppressing catastrophe, whereas, in contrast, EB2 does not play a direct role in microtubule dynamic instability, and little is known about the cellular function of EB2. By quantitative proteomics, we identified mammalian HCLS1-associated protein X-1 (HAX1) as an EB2-specific interacting protein. Knockdown of *HAX1* and *EB2* in skin epidermal cells stabilizes focal adhesions and impairs epidermal migration *in vitro* and *in vivo*. Our results further demonstrate that cell motility and focal adhesion turnover require interaction between Hax1 and EB2. Together, our findings provide new insights for this critical cellular process, suggesting that EB2 association with Hax1 plays a significant role in focal adhesion turnover and epidermal migration.

Cell migration is an essential process for developmental morphogenesis, wound healing, and tumor metastasis. The intricate, multistep process of cell migration requires integrated activities of the cytoskeleton, membrane, and cell/extracellular matrix adhesions (1, 2). During the process, focal adhesion plays a critical role in establishing a connection between the extracellular matrix and the actin cytoskeleton and serves as a point of traction for the cell (1, 3–6).

Microtubules are polar filaments with two structurally and functionally distinct ends, the plus end and the minus end. Interestingly, it has been well documented that microtubules can target peripheral focal adhesions (7–10), a process mediated by the mammalian spectraplakin protein ACF7 (11, 12). Furthermore, accumulating evidence has shown that the growth of microtubules can promote focal adhesion turnover by serving as tracks to deliver proteins essential for focal adhesion disassembly (7–10). For example, recently, a mitogen-activated protein kinase kinase kinase kinase 4 (MAP4K4)[2] has been identified as a focal adhesion regulator that associates with microtubules. Knockout of *MAP4K4* stabilizes focal adhesions and impairs cell migration (13).

Microtubule plus end tracking proteins are a diverse group of evolutionarily conserved proteins that enrich at the growing ends (plus ends) of microtubules (14, 15). Plus end proteins have been shown to participate in different aspects of cell architecture through their function in regulating microtubule dynamics and the interaction of microtubules with other cellular structures. It has been established that the three microtubule end-binding proteins (EB1, EB2, and EB3) in mammalian cells can track the plus ends of growing microtubules. They also share substantial sequence homology. EB1 and EB3 together can regulate microtubule dynamics by promoting microtubule growth and suppressing catastrophe, whereas, in contrast, EB2 does not play a direct role in microtubule dynamic instability, and little is known about the cellular function of EB2 (16, 17). Interestingly, our recent work has demonstrated that EB2 plays an essential role in the regulation of focal adhesion dynamics and cell migration via its interaction with MAP4K4 (13).

To dissect the roles of different EB proteins during cell motility, we determined the interactomes of EB1, EB2, and EB3 by a quantitative proteomics approach (18, 19). Our MS analysis revealed an intriguing interaction partner, HAX1, which is specifically associated with EB2 but not EB1 or EB3. Hax1 was initially identified as a binding partner of HS1, the hematopoietic homologue of cortactin (20). It has been suggested that deficiency in *Hax1* leads to neutropenia by regulating neutrophil apoptosis (21). However, Hax1 is actually a ubiquitous protein that regulates the actin cytoskeleton and cell migration. Hax1 has been shown to associate with various cell adhesion molecules, including β6 integrin, cortactin, and HS1 (22, 23). Most interestingly, it has been shown that loss of *Hax1* in neutrophils enhances integrin-mediated cell adhesion, strongly suggesting that Hax1 is critically involved in cell adhesion dynamics (24).

Mammalian skin provides a versatile and accessible platform to investigate cytoskeletal dynamics and cell migration *in vivo* (12, 25, 26). Impaired movement of epidermal cells can delay skin wound healing and have dire consequences for animal sur-

* This work was supported by National Institutes of Health Grant R01-AR063630, American Cancer Society Research Scholar Grant RSG-13-198-01, and the V Scholar Award from the V Foundation (to X. W.). The authors declare that they have no conflicts of interest with the contents of this article. The content is solely the responsibility of the authors and does not necessarily represent the official views of the National Institutes of Health.

[S] This article contains supplemental Tables 1–3 and Movies 1–4.

[1] To whom correspondence should be addressed: University of Chicago, GCIS W408B, 929 E 57th St., Chicago, IL 60637. Tel.: 773-702-1110; Fax: 773-702-4476; E-mail: xiaoyangwu@uchicago.edu.

[2] The abbreviations used are: MAP4K4, mitogen-activated protein kinase kinase kinase kinase 4; EB, end-binding; TIRF, total internal reflection fluorescence microscopy.

vival. In this report, we found that knockdown of *HAX1* or *EB2* in skin keratinocytes leads to aberrant focal adhesion dynamics and impaired cell migration. With a skin grafting model, we further show that both HAX1 and EB2 play an essential role in skin wound healing and epidermal migration *in vivo*. Taken together, our study unravels an important mechanism whereby microtubule plus ends regulate focal adhesion turnover and directional cell movement through interaction between EB2 and Hax1.

Experimental Procedures

Stable Isotope Labeling by Amino Acids in Cell Culture and LC-MS/MS Analysis—HEK293T cells were labeled with either "heavy" or "light" isotopic lysine using a stable isotope labeling by amino acids in cell culture protein quantification kit (Thermo Scientific, Rockford, IL) according to the instructions of the manufacturer. Briefly, cells were grown in DMEM:F12 medium supplemented with 10% dialyzed fetal bovine serum and either the heavy form of L-lysine-2HCl (4,4,5,5-D4) or light L-lysine for more than six generations to achieve more than 98% labeling efficiency (19). Cells were transiently transfected with expression vectors encoding N-terminal triple HA-tagged EB1, EB2, EB3, or GST as a "spike-in" control.

Protein lysates were subjected to purification with an α-HA affinity column, and nonspecific binding proteins were washed off with washing buffer containing increasing amount of salts. Protein bands were excised by sterile razor blade and chopped into $\sim$1-mm^3 pieces. MS analysis was carried out by the proteomics core of the University of Chicago. Each sample was washed in water and destained using 100 mM ammonium bicarbonate (pH 7.5) in 50% acetonitrile. A reduction step was performed by addition of 100 μl of 50 mM ammonium bicarbonate (pH 7.5) and 10 μl of 10 mM Tris(2-carboxyethyl)phosphine HCl at 37 °C for 30 min. The proteins were alkylated by adding 100 μl of 50 mM iodoacetamide and allowed to react in the dark at 20 °C for 30 min. Gel samples were washed in water, then in acetonitrile, and dried in a SpeedVac. Trypsin digestion was carried out overnight at 37 °C with a 1:50 enzyme:protein ratio of sequencing grade-modified trypsin (Promega) in 50 mM ammonium bicarbonate (pH 7.5) and 20 mM $CaCl_2$. Peptides were extracted with 5% formic acid and vacuum-dried.

The peptide samples were loaded to a 0.25-μl C_8 OptiPak trapping cartridge custom-packed with Michrom Magic C8 (Optimize Technologies), washed, and then switched in-line with a 20 cm $\times$ 75 μm C_{18} packed spray tip nanocolumn packed with Michrom Magic C18AQ for a two-step gradient. Mobile phase A was water/acetonitrile/formic acid (98/2/0.2), and mobile phase B was acetonitrile/isopropanol/water/formic acid (80/10/10/0.2). Using a flow rate of 350 nl/min, a 90-min, two-step LC gradient was run from 5% B to 50% B in 60 min, followed by 50–95% B over the next 10 min, hold for 10 min at 95% B, back to starting conditions, and re-equilibrated. The samples were analyzed via LC-MS/MS on a Q-Exactive (Thermo Scientific) mass spectrometer using a 60,000 reversed phase survey scan, m/z 375–1950, with lockmasses, followed by 15 higher-energy collisional dissociation collision-induced dissociation scans on only doubly and triply charged precursors between 375 Da and 1950 Da. Inclusion lists of expected acetylated or phosphorylated tryptic *in silico* peptide ion masses were also used. Ions selected for MS/MS were placed on an exclusion list for 60 s.

Tandem mass spectra were extracted by MSConvert (ProteoWizard 3.0.3768) All MS/MS samples were analyzed using MaxQuant (Max Planck Institute of Biochemistry, Martinsried, Germany; version 1.2.2.5. MaxQuant was set up to search the 140204_SPROT_HUMAN database (unknown version, 47496 entries) also assuming strict trypsin. MaxQuant and X! Tandem were searched with a fragment ion mass tolerance of 20 parts per million and a parent ion tolerance of 20 PPM. Carbamidomethyl of cysteine was specified in MaxQuant as a fixed modification. Label:2H(4) of lysine, oxidation of methionine, acetyl of the N terminus, and phospho of serine, threonine, and tyrosine were specified in MaxQuant as variable modifications.

Antibodies, Reagents, and Plasmid DNA Constructions—The mouse monoclonal antibody against HAX1 was obtained from BD Biosciences. The rat monoclonal antibody against EB2 was obtained from Thermo (Waltham, MA). Human plasma fibronectin, HA-conjugated agarose, mouse monoclonal Vinculin, and β-tubulin antibodies were obtained from Sigma. Mouse monoclonal antibodies against Myc and rabbit polyclonal antibodies against HA were obtained from Santa Cruz Biotechnology, Inc. (Santa Cruz, CA). Other chemicals or reagents were obtained from Sigma unless indicated otherwise.

Plasmids encoding DsRed-Zyxin, GFP-paxillin, and EB2 have been described previously (11, 27). Full-length *HAX1* cDNA was gBlocked from IDT (Coralville, IA) and cloned into the mammalian expression vectors pKH3S and pHANS (with an N-terminal HA or Myc tag). The plasmid encoding full-length *EB2* cDNA was a gift from Dr. Yulia Komarova (University of Illinois at Chicago). The *EB2* coding sequence was subcloned to other mammalian expression vectors, including pKH3. Mutations in *HAX1* were created by the following primers: GCG GGA TCC ATG AGC CTC TTT GAT CTC TTC CG, CGG AAT TCC TAC TCT GAC TCA GGA CCT GGA AG; GCG GGA TCC ATG ACA CCT GGT GAG AGA CTA CGG, CGG AAT TCC TAC CGG GAC CGG AAC CAA C; GCG GGA TCC GAT GAC ACC TGG TGA GAG ACT ACG G; CGG AAT TCC TAG GCT GGA GGT CTT GGT GAT TC; CGG AAT TCC TAT CTG GTT CTA GGA TGG GGG TC; GCG GGA TCC ATG GAG GAC AAT GAT CTT GAT TCC. ShRNA vectors targeting *HAX1* were prepared from the Decipher shRNA vector (pRSI9-U6-UbiC-TagRFP-2A-Puro) with the following primers: aCC GGG CAG ACA CTA CGA GAC TCA ATC TCG AGA TTG AGT CTC GTA GTG TCT GCT TTT TG, cga aCA AAA AGC AGA CAC TAC GAG ACT CAA TCT CGA GAT TGA GTC TCG TAG TGT CTG Cc; aCC GGC CAG CCC AAA TCG TAT TTC AAC TCG AGT TGA AAT ACG ATT TGG GCT GGT TTT TG, cga aCA AAA ACC AGC CCA AAT CGT ATT TCA ACT CGA GTT GAA ATA CGA TTT GGG CTG Gc; aCC GGT CAG CTT TGG ATG ATC CCT TTC TCG AGA AAG GGA TCA TCC AAA GCT GAT TTT TG, cga aCA AAA ATC AGC TTT GGA TGA TCC CTT TCT CGA GAA AGG GAT CAT CCA AAG CTG Ac. The mutation at the *EB2* shRNA recognition site was created by overlapping PCR with the following primers: AGC ATC CTT TAA ACG GAT GAA CGT CGA CAA AGT CAT CCC AGT GGA GAA G, CTT CTC CAC TGG GAT GAC TTT GTC

GAC GTT CAT CCG TTT AAA GGA TGC T. The mutations in *EB2* were created by overlapping PCRs with the following primers: AAG GAA AAA AGC GGC CGC TCA TGG CGG TCA ATG TGT ATT CTA C, GGA ATT CTT AAT ACT CTT CTT GTT CCT CCT GTG GGC CCC CTT CAT CAG GTA TCA CAA AGC CTT CAT CGG AAG CGT AGA GCA C, TCC TAA GGC TGG CCC CGG AAT GGT GCG AAA GAA TCC TGG TGT GGG CAA TGG AGA TGA TGA AGC AGC TGA ACT CAA CGA GCA GGT ACA TTC, CCA CAG AGA CCC ATT GCA ACA CAG AGG ACT ACT GCA GCT CCT AAG GCT GGC CCC GGA ATG, GAA GAT CTT CAA CCT GCC CAA GAA GCC TCT CGG CTC CAG TAC TGC AGC CCC ACA GAG ACC CAT TGC AAC. For the EB2/EB1 swapping mutant, the internal region close to the coiled-coil domain from EB2 (amino acid sequence SHHANSPTAGAAKSSPASKPGS-TPSRPSSAKRASSSGSASRSDKDLETQVIQ) was changed to the corresponding sequence from EB1 (PLGSSTAAPQRPIAT-QRTTAAPKAGPGMVRKNPGVGNGDDEAAE), or the acidic C terminus of EB2 (QEGQTEEPEAEEQAHDQQPQQQEEY) was changed to the corresponding sequence from EB1 (GFV-IPDEGGPQEEQEEY).

Skin Grafting and Wound Healing—All mice used in this study were bred and maintained at the Animal Resource Center of the University of Chicago in accordance with institutional guidelines.

Skin grafting was carried out essentially as described previously (28). Briefly, dermis was prepared from newborn skin, and primary keratinocytes were seeded onto the dermis and cultured. Skins were then grafted on the back of adult nude mice. For skin wound healing assays, nude mice were anesthetized, and two full-thickness excisional wounds were made on both sides of the dorsal midline (28) where skins were grafted. Mice were housed separately, and no self-induced trauma was observed in mice. Tissue was collected 2–6 days after wounding, and wound re-epithelialization was evaluated by histological analyses. Hyperproliferative epidermis was identified by hematoxylin and eosin staining, and the length of the hyperproliferative epidermis that extended into the wounds was measured and quantified.

Histology and Immunofluorescence—Skin or wound samples were embedded in optimal cutting temperature, frozen, sectioned, and fixed in 4% formaldehyde. For paraffin sections, samples were incubated in 4% formaldehyde at 4 °C overnight, dehydrated with a series of increasing concentrations of ethanol and xylene, and then embedded in paraffin. Paraffin sections were rehydrated in decreasing concentrations of ethanol and subjected to antigen unmasking in 10 mM citrate (pH 6.0). Sections were subjected to hematoxylin and eosin staining or immunofluorescence staining as described previously (28). Antibodies were diluted according to the instructions of the manufacturer unless indicated otherwise.

For immunofluorescence staining of cultured keratinocytes, cells were fixed in 4% formaldehyde and then permeabilized in 0.5% Triton solution. Processed cells were subjected to immunostaining as described previously (28). For staining of EB2 and microtubules, an optimized staining procedure was used to preserve microtubule structure. Cells were fixed in microtubule fixation buffer containing 80 mM PIPES (pH 6.9), 50 mM NaCl, 2 mM $MgCl_2$, 0.4 mM $CaCl_2$, 1% glutaraldehyde, 3% paraformaldehyde, 0.2% Triton X-100. Autofluorescence of glutaraldehyde was quenched by treatment of $NaBH_4$ after staining. Stained cells were subjected to imaging with confocal or TIRF microscopy.

Cell Culture and Transfections—Primary mouse keratinocytes were isolated from the epidermis of newborn mice using trypsin after prior separation of the epidermis from the dermis by an overnight dispase treatment. Keratinocytes were plated on mitomycin C-treated 3T3 fibroblast feeder cells until passage 3. Cells were cultured in E-medium supplemented with 15% serum and a final concentration of 0.05 mM Ca^{2+}. All experiments were performed using primary cells with less than 10 passages.

For transient transfections, primary keratinocytes were transfected with FuGENE6 according to the protocol of the manufacturer. Cells were usually examined 24–48 h post-transfection.

Cell Migration Assays and Time-lapse Video Microscopy—The scratch wound healing assay was performed essentially as described previously (12). Briefly, keratinocytes were plated on 35-mm tissue culture dish coated with fibronectin. After cells reached confluency, wounds were created by manual scraping of the cell monolayer with a pipette tip. The dishes were then washed with PBS, replenished with media, and photographed using a phase-contrast microscope. Afterward, dishes were placed in the tissue culture incubator, and the matched wound regions were photographed 12 and 24 h after wounding. To trace the movement of individual keratinocytes, cells were plated on fibronectin-coated dishes and imaged with an Olympus phase-contrast microscope (×20) for 3 h at 2 frames/min and tracked manually in ImageJ.

Focal Adhesion Assembly/Disassembly Measurements—Kinetics of focal adhesion assembly and disassembly were performed essentially as described previously (12). Keratinocytes were plated on fibronectin-coated dishes and transfected with a plasmid encoding GFP-paxillin. Time series of images were acquired on a spinning disc confocal microscope equipped with a ×100 α-plane (1.45 oil) lens and an EM charge-coupled device camera. The rate constants for focal adhesion assembly and disassembly were obtained by calculating the slope of relative fluorescence intensity increases or decreases of individual focal adhesion on a semilogarithmic scale against time.

Western Blots—Western blotting was performed as described previously (12). Briefly, equal amounts of the cell lysates were separated on a 12% SDS-PAGE and electroblotted onto an nitrocellulose membrane. The immunoblot was incubated with Odyssey blocking buffer (Li-Cor) at room temperature for 1 h, followed by overnight incubation with primary antibody. Blots were washed three times with Tween 20/Tris-buffered saline (TBST) and incubated with a 1:10,000 dilution of secondary antibody for 1 h at room temperature. Blots were again washed three times with TBST. Visualization and quantification was carried out with the Li-Cor Odyssey scanner and software (Li-Cor Biosciences).

Statistical Analysis—Statistical analysis was performed using Excel or OriginLab software. Box plots are used to describe the entire population without assumptions on the statistical distri-

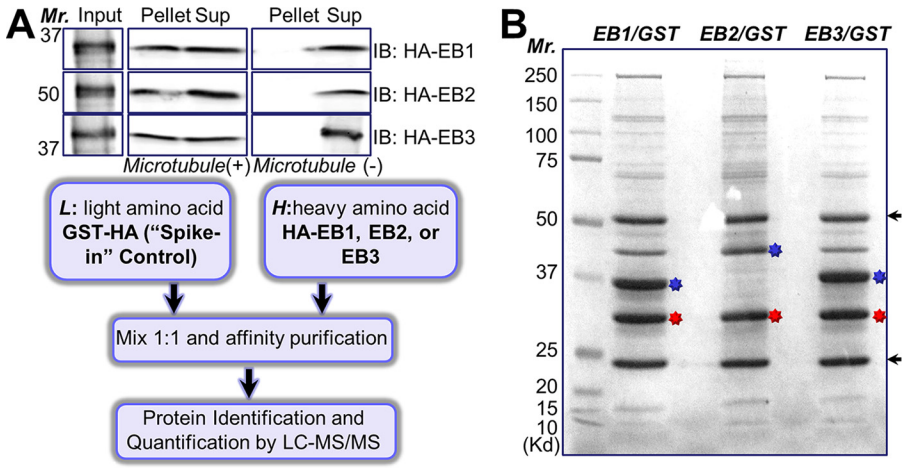

C

Gene Name	EB1/GST	EB2/GST	EB3/GST
MAPRE1 (EB1)	/	23.47	18.56
MAPRE2 (EB2)	27.04	/	24.85
MAPRE2 (EB3)	20.88	47.77	/
KIF2C	6.34	12.09	N/I
DCTN1	4.94	9.38	N/I
SURF6	4.73	1.10	N/I
HAX1	N/I	19.32	N/I
CDC7	N/I	11.83	N/I
ABCF2	N/I	11.06	N/I

(Log_2*Heavy/Light*)

FIGURE 1. **Identification of Hax1 as an EB2-specific binding partner.** *A*, *top panel*, interaction of HA-tagged EB1, EB2, and EB3 with microtubules was examined by co-sedimentation assay. The presence of proteins in the original lysate (*Input*), pellet of ultracentrifugation, as well as the supernatant (*Sup*) was determined by immunoblot (*IB*) with α-HA antibodies. *Bottom panel*, flow diagram of the protocol used to isolate EB binding proteins for stable isotope labeling by amino acids in cell culture analysis. *B*, control (GST) or different EB proteins and their associated proteins were isolated by tandem affinity purification and resolved by SDS-PAGE. The IgG heavy chain and light chain are marked by *arrows*. The putative bands for EB1, EB2, and EB3 are marked by *blue stars*, and GST in the same lane is marked by *red stars*. *C*, candidate binding partners of different EB proteins that exhibit most significant changes in $\log_2$(heavy/light). Note that multiple candidates (*red*), including Hax1, are only present in the purification of the EB2 complex.

bution. Student's *t* test was used to assess the statistical significance (*p* value) of differences between two experimental conditions.

Results

Identification of HAX1 as an EB2-specific Binding Partner—Mammalian cells express three EB proteins (EB1, EB2, and EB3), among which the function of EB2 remains most unclear. To dissect the cellular function of different EB molecules, we engineered expression vectors encoding triple HA-tagged EB1, EB2, and EB3. The presence of N-terminal HA tags does not affect EB protein association with microtubules (Fig. 1*A*). We used affinity purification to isolate different EB complexes from transfected cells, and then employed stable isotope labeling by amino acids in cell culture coupled with LC-MS/MS to determine the interactome of each EB protein (Fig. 1, *A* and *B*). With GST as a common spike-in control, our quantitative proteomics revealed multiple binding partners for each EB molecule (Fig. 1*C* and supplemental Tables 1–3). Interestingly, in addition to EB proteins themselves (heterodimerization) and microtubule motor molecules, EB2 interacts with far more binding partners than EB1 or EB3. With a cutoff log2 ratio (heavy/light) of more than 2, we identified ~90 binding proteins for EB2, whereas EB1 and EB3 had less than 10 specific binding partners in our analysis (supplemental Tables 1–3). These results are consistent with our previous hypothesis that EB2 may act as a microtubule adaptor protein to recruit functional cargo molecules to the plus ends of growing microtubules (13).

Of all identified EB2 binding partners, Hax1 is particularly interesting to us. Our proteomics results suggest that it is an EB2-specific binding protein because the same protein was not retrieved from EB1 or EB3 pulldowns. Hax1 has a log2 (heavy/light) ratio of 19.32, suggesting high-affinity association with

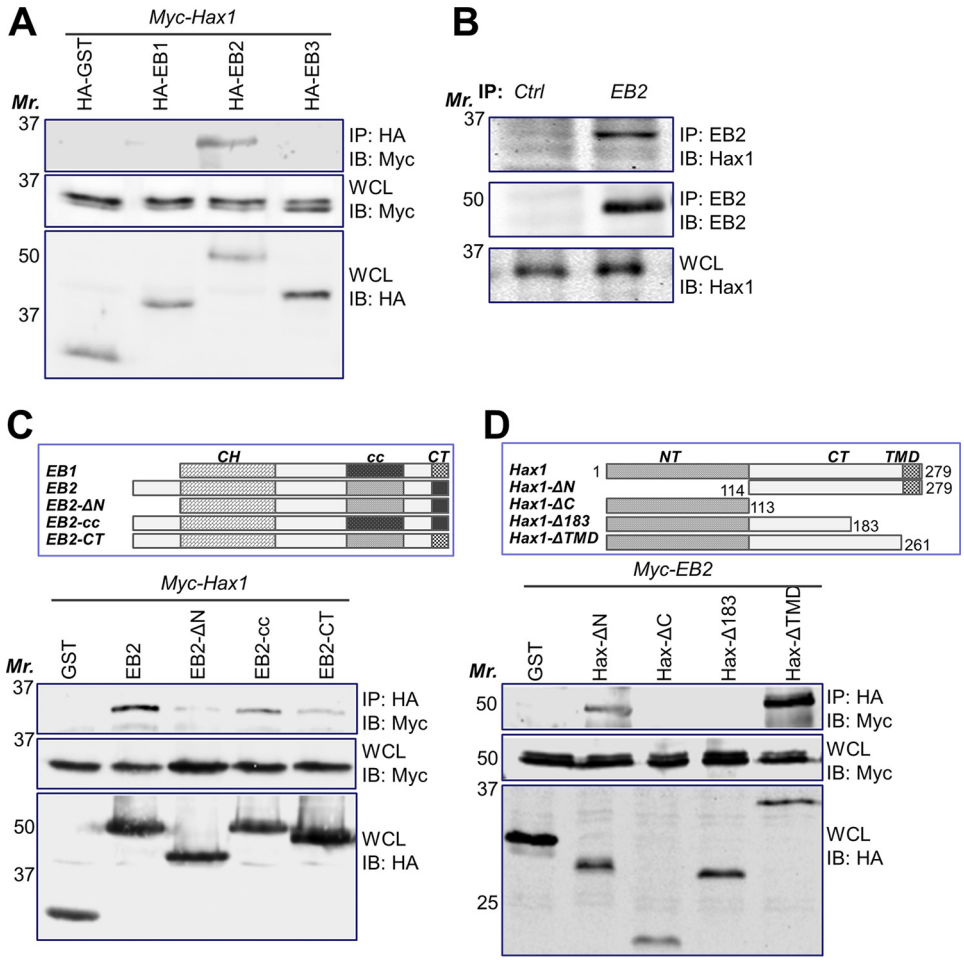

FIGURE 2. **EB2 interaction with Hax1.** *A*, HEK293T cells were transfected with different plasmids as indicated. Cell lysates were immunoprecipitated (*IP*) with α-HA antibody and immunoblotted (*IB*) with different antibodies as indicated. For whole-cell lysate (*WCL*), 10 μg of total protein was used. Note that only EB2 specifically pulls down Hax1. *B*, keratinocyte lysate was immunoprecipitated with α-EB2 or control (*Ctrl*) antibodies. The immunoprecipitate and whole-cell lysate (10 μg of total protein) were subjected to immunoblot with different antibodies as indicated. *C*, *top panel*, schematic of EB1, EB2, and various EB2 mutants used for coimmunoprecipitation assays. *Bottom panel*, the association of EB2 or EB2 mutants with Hax1 was determined by coimmunoprecipitation as described above. For whole-cell lysate, 10 μg of total protein was used. *CH*, calponin homology domain; *cc*, coiled-coil domain; *CT*, acidic C terminus. *D*, *top panel*, schematic of Hax1 and various Hax1 mutants used for coimmunoprecipitation assays. *Bottom panel*, the association of different Hax1 mutants with EB2 was determined by coimmunoprecipitation as described above. For whole-cell lysate, 10 μg of total protein was used. *NT*, N terminus; *CT*, C terminus; *TMD*, transmembrane domain.

EB2. More importantly, previous studies have demonstrated a potential role of Hax1 in cell adhesion (22–24), which is consistent with the function of EB2 in the regulation of focal adhesion dynamics and cell motility. To verify the interaction between HAX1 and EB2, we co-expressed Hax1 with EB1, EB2, or EB3. Immunoprecipitation results suggest that Hax1 only associates with EB2 but not EB1 or EB3, as expected (Fig. 2*A*). We also carried out endogenous co-immunoprecipitation assays and detected a significant amount of EB2 in HAX1 immunoprecipitates but not in the control samples (Fig. 2*B*).

EB family members share significant sequence similarity. Alignment of three EB family members suggests three unique regions in EB2, the N terminus, the acidic C terminus (*CT*), and an internal region close to the coiled-coil (*cc*) domain (Fig. 2*C*). To examine their contribution to binding with Hax1, we introduced deletion or swapping mutations to *EB2* by either removing the N terminus or replacing the different regions in *EB2* with corresponding sequences from *EB1* (Fig. 2*C*). We then carried out co-immunoprecipitation assays to determine their respective binding affinities to Hax1. Our results show that changes in any of the three regions lead to a significant reduction in Hax1 binding, whereas N terminus deletion almost abolished Hax1 interaction (Fig. 2*C*). These results suggest that Hax1 may associate with multiple regions in EB2, with the N terminus of EB2 harboring the most critical binding determinants.

To further characterize Hax1 interaction with EB2, we generated different truncation mutants of Hax1. Co-immunoprecipitation analysis showed that a C-terminal part other than the N-terminal part of HAX1 is necessary for the interaction with EB2 (Fig. 2*D*). To narrow down the potential domain involved in the interaction between HAX1 and EB2, we further generated and examined different HAX1 C-terminal deletion mutants on the basis of previous literature (22–24), including the Δ183 mutant (deletion of the C-terminal 97 residues that include the potential transmembrane domain) and ΔTMD (deletion of 18 residues at the transmembrane domain) mutant. Co-immunoprecipitation results show that Δ183, but not ΔTMD,

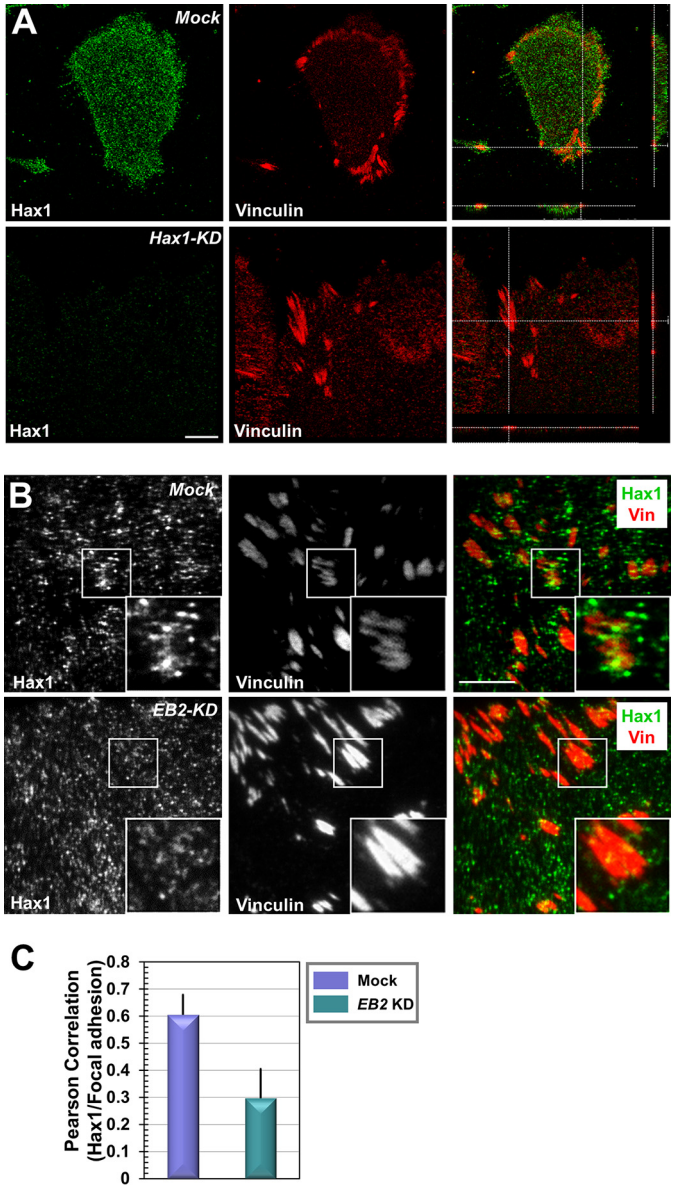

FIGURE 3. **Hax1 localizes at focal adhesions in an EB2-dependent manner.** *A*, immunofluorescence staining for Hax1 (*green*) and vinculin (*red*) in mock keratinocytes or Hax1 knockdown (*KD*) cells. Cells were imaged by confocal microscopy. The *right panels* are merged images with corresponding cross-sections (*dashed lines*) showing three-dimensional stacks. *Scale bar* = 20 μm. *B*, immunofluorescence staining for Hax1 (*green*) and focal adhesion (*Vin*, vinculin; *red*) in mock or *EB2* knockdown keratinocytes. Cells were imaged by TIRF microscopy. The *boxed areas* are magnified as *insets*. *Scale bar* = 20 μm. *C*, co-localization of Hax1 and focal adhesions (vinculin) was determined by Pearson correlation coefficient (n = 20 cells for each). Note that Hax1 localization at focal adhesions is reduced significantly in EB2-depleted cells (Student's t test, $p < 0.01$).

abolished EB2 interaction (Fig. 2*D*), suggesting that the corresponding C-terminal region is essential for EB2 binding.

Hax1 has been shown to regulate integrin-based cell adhesion in neutrophils (24). To test subcellular localization of Hax1, we carried out immunofluorescence staining of endogenous Hax1 together with focal adhesions in cultured primary keratinocytes. Confocal imaging of stained keratinocytes indicates a punctate localization of Hax1 at the ventral surface of the cell, with enriched staining at the cell periphery, where focal adhesions localize (Fig. 3*A*; the complete Z stacks of the confocal images are shown in supplemental Movies 1 and 2). Staining of Hax1-depleted cells with the same antibody shows strongly diminished signals, supporting the specificity of our staining procedures (Fig. 3*A* and supplemental Movies 3 and 4). To specifically image Hax1 localization at cell adhesions and suppress the signals from cytosolic Hax1, we employed total internal reflection fluorescence microscopy (TIRF), which can selectively illuminate and excite fluorophores in the restricted region immediately adjacent to the cell-contacting surface (29). With TIRF microscopy, our staining shows significant enrichment of Hax1 around focal adhesions in WT keratinocytes, and depletion of *EB2* disrupts this colocalization (Fig. 3*B*; quantification in Fig. 3*C*).

Our recent study has demonstrated the potential role of EB2 as an adaptor molecule to deliver key proteins through microtubules for regulation of focal adhesion dynamics (13). To determine the localization of EB2 and Hax1 in keratinocytes, we imaged both endogenous and exogenously expressed Hax1 and EB2 with TIRF microscopy. Because microtubule network and EB2 staining are sensitive to fixation, we examined the localization of Hax1 and EB2 under different conditions. Our results demonstrate colocalization between Hax1 and EB2 in both formaldehyde-fixed (Fig. 4*A*) and glutaraldehyde-fixed (Fig. 4*B*) keratinocytes. In addition, transiently expressed Hax1 and EB2 display a similar colocalization under TIRF (Fig. 4*B*).

To test the potential association between Hax1 and microtubules, we performed microtubule pulldown assays. Our data indicate microtubule association of Hax1 in WT cells but not in EB2-depleted cells (Fig. 4*C*). Depletion of Hax1 in cultured keratinocytes, however, does not affect EB2 association with microtubules (Fig. 4*C*). Together, our results suggest that EB2 can recruit Hax1 to microtubule growing ends and focal adhesions through its interaction with Hax1.

EB2 and Hax1 Interaction Is Essential for Epidermal Cell Migration—Our previous work established an important role of EB2 in regulation of focal adhesion turnover and cell motility (13). To examine whether EB2 and Hax1 interaction contributes to cell movement, we first monitored cell migration with EB2 and Hax1 knockdown keratinocytes. When introducing an ~500-μm scratch wound into the cell monolayer, EB2 and Hax1 knockdown cells both displayed a significant delay in the recovery of these scratches (Fig. 5, *A* and *B*). BrdU incorporation analysis shows comparable cell proliferation in control cells or cells depleted of *EB2* or *Hax1* (Fig. 5*B*), strongly suggesting that the delayed wound healing is likely due to cell movement defects. Video microscopy permitted imaging and monitoring the velocities of individual keratinocytes (Fig. 5*C*). Depletion of endogenous Hax1 or EB2 by shRNA leads to significant inhibition of cell motility (Fig. 5, *C* and *D*). Re-expression of exogenous EB2 or Hax1 in the corresponding knockdown cells can restore cell motility. However, expression of an EB2 mutant deficient for Hax1 interaction (EB2-ΔN) or a Hax1 mutant defective in EB2 interaction (Hax1-ΔC183) failed to recover the motility defect, strongly suggesting that EB2 and Hax1 interaction plays an essential role in cell migration.

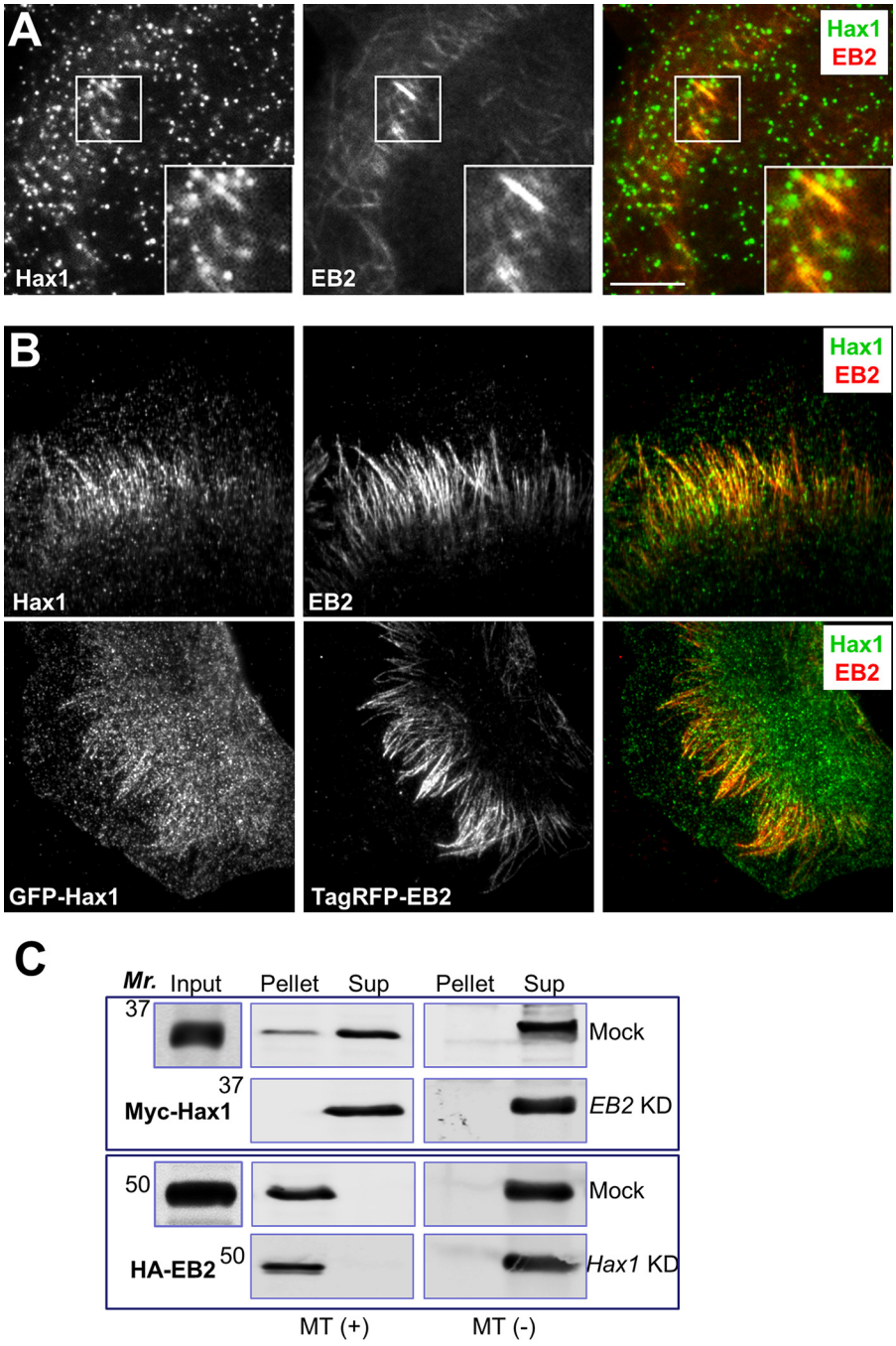

FIGURE 4. **EB2 recruits Hax1 to microtubules.** *A*, immunofluorescence staining for Hax1 (*green*) and EB2 (*red*) in primary mouse skin keratinocytes fixed with a conventional procedure (formaldehyde). Stained cells were imaged by TIRF microscopy. The *boxed areas* are magnified as *insets*. *Scale bar* = 20 μm. *B*, immunofluorescence staining for endogenous Hax1 (*green*) and EB2 (*red*, *top panels*) or exogenously expressed Hax1 and EB2 in mouse keratinocytes fixed with glutaraldehyde. Stained cells were imaged by TIRF microscopy. *C*, the interaction with microtubules (*MT*) was examined by co-sedimentation assay. The presence of proteins in the original lysate (*Input*), pellet of ultracentrifugation, as well as the supernatant (*Sup*) was determined by immunoblot with different antibodies as indicated. *KD*, knockdown.

EB2 and Hax1 Interaction Regulates Focal Adhesion Dynamics—To determine the role of EB2/Hax1 interaction in focal adhesion dynamics, we first examined cell/extracellular matrix adhesions after *EB2* or *Hax1* depletion. Immunofluorescence microscopy showed significantly enhanced labeling of focal adhesion in *EB2* or *Hax1* knockdown keratinocytes relative to controls (Fig. 6*A*). Quantification of the presence of Vinculin showed a significant increase in the size of focal adhesions in the two knockdown lines. To further examine the role of HAX1/EB2 association in focal adhesion dynamics, we employed confocal video microscopy to trace and examine the behavior of individual focal adhesion in knockdown cells. To monitor this process, we transfected cells with plasmids encoding GFP-paxillin. Representative examples of the perturbations in focal adhesions dynamics arising from HAX1 depletion are shown in montages in Fig. 6*B*. During the interval of observation, focal adhesions in control keratinocytes usually underwent continuous bouts of formation, maturation, and disassembly, whereas focal adhesion in EB2- or Hax1-

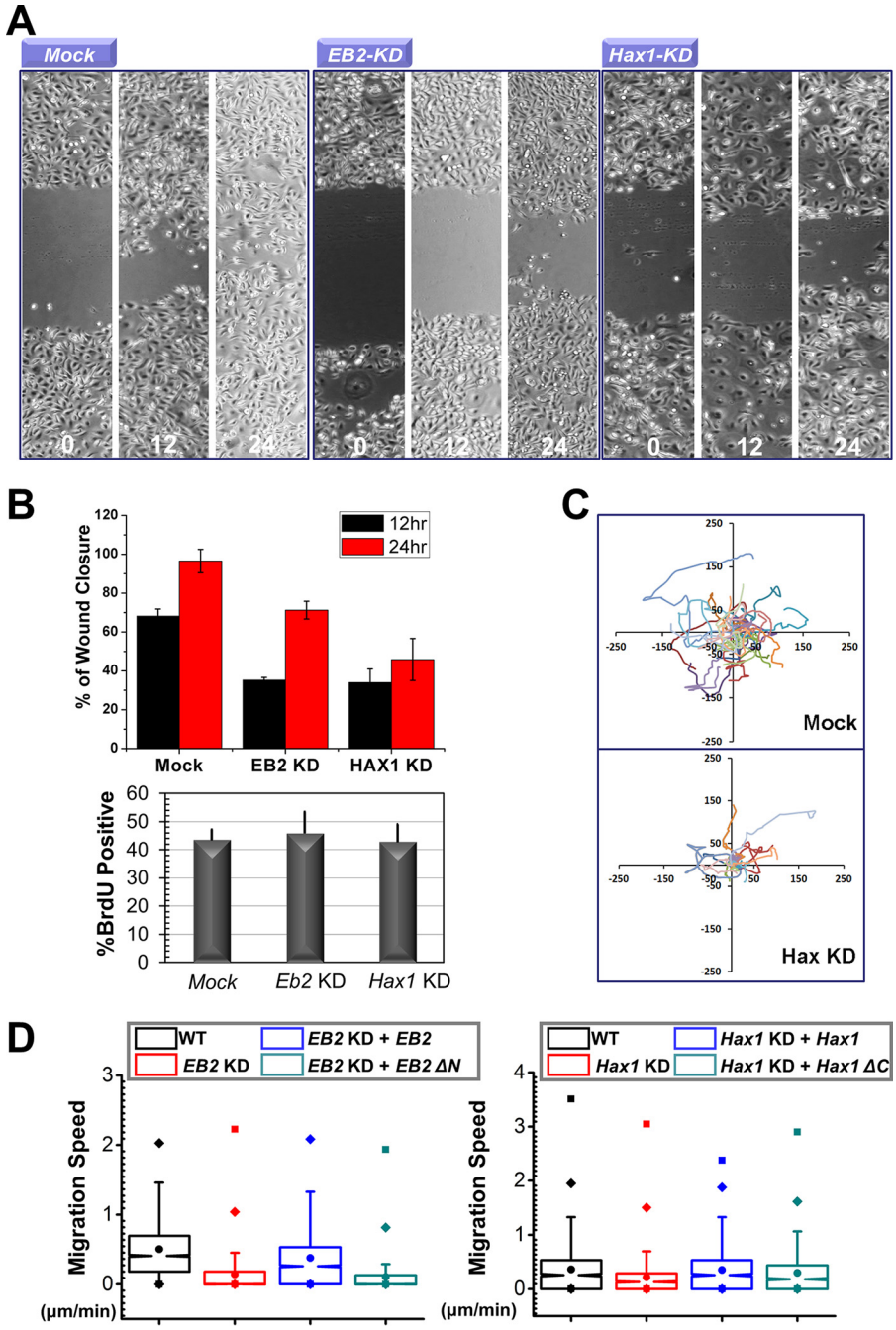

FIGURE 5. **EB2/Hax1 interaction regulates cell migration.** A and B, the migration of confluent monolayers of mouse keratinocytes cultured from WT (*Mock*), EB2-depleted, or Hax1-depleted cells was assessed by *in vitro* scratch wound assays (*A*). The kinetics of *in vitro* wound healing are quantified in *B*. Note that knockdown (*KD*) of EB2 or Hax1 leads to significant inhibition of *in vitro* wound healing ($n = 3$, $p < 0.01$, Student's *t* test). Cell proliferation *in vitro* was examined by BrdU incorporation assay. Statistical analysis with Student's *t* test showed that knockdown of EB2 or Hax1 did not significantly affect cell proliferation compared with the mock sample ($n = 3$, $p > 0.1$). *C*, movements of individual keratinocytes were traced by video microscopy. The migration tracks of multiple cells for each group (mock or Hax1 knockdown) are shown here as scatter plots ($n = 30$). *D*, cell motility for WT or different knockdown cells or knockdown cells (30 cells for each) rescued with EB2 or Hax1 were quantified with ImageJ and are shown as box and whisker plots (box and whisker plots indicates the mean (*empty square within the box*), 25th percentile (*bottom line of the box*), median (*center line of the box*), 75th percentile (*top line of the box*), 5th and 95th percentiles (*whiskers*), first and 99th percentiles (*solid diamonds*), and minimum and maximum measurements (*solid squares*). Statistical analysis with Student's *t* test showed that knockdown of EB2 or Hax1leads to a significant decrease in speed compared with mock cells ($p < 0.01$). Re-expression of WT *EB2* or *Hax1* but not their corresponding mutants leads to a significant increase in migration speed compared with the knockdown cells ($p < 0.01$).

depleted cells were significantly more static. Quantifications of the kinetics of individual focal adhesions revealed dramatic decrease in the disassembly rates of focal adhesions in knockdown cells (Fig. 6*C*). Exogenous expression of WT EB2 or Hax1 in the corresponding knockdown cells can restore focal adhesion turnover, whereas the EB2 mutant deficient for Hax1 interaction (EB2-ΔN) or the Hax1 mutant defective in EB2 interaction (Hax1-ΔC183) cannot (Fig. 6*C*). Together, our results provide compelling evidence that EB2 interaction with Hax1 plays a critical role in focal adhesion dynamics.

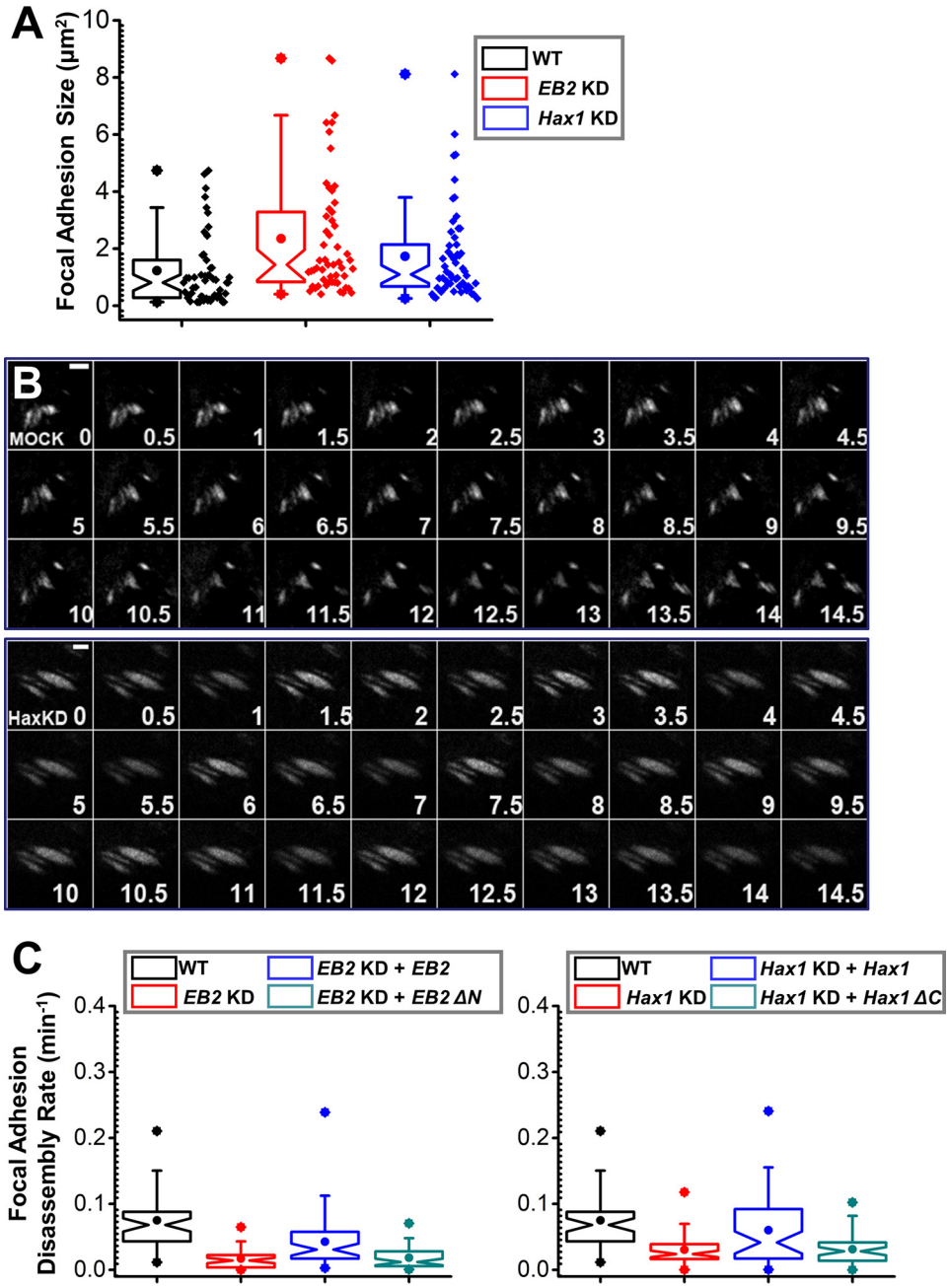

FIGURE 6. **EB2 interaction with Hax1 regulates focal adhesion dynamics *in vitro*.** *A*, box and whisker plot indicating the size distribution of focal adhesions in WT or EB2 or Hax1 knockdown (*KD*) cells (~50 focal adhesions were analyzed for each genotype). Statistical analysis with Student's *t* test showed that knockdown of EB2 or Hax1leads to a significant increase in focal adhesion size compared with mock cells ($p < 0.01$). *B*, representative time-lapse images (montages) of GFP-paxillin-expressing keratinocytes. Note the formation and dissolution of focal adhesions in WT cells and very static focal adhesion in hax1 knockdown cells. *Scale bars* = 10 μm. *C*, box and whisker plots revealing slow disassembly rates of focal adhesions in EB2 or Hax1 knockdown cells relative to their WT counterparts. EB2 but not the EB2 mutant and Hax1 but not the Hax1 mutant can rescue the defect in focal adhesion dynamics when introduced to express exogenously in the corresponding knockdown cells. For each genotype, ~50 focal adhesions were analyzed. Statistical analysis with Student's *t* test showed that knockdown of EB2 or Hax1leads to a significant decrease of focal adhesion disassembly compared with mock cells ($p < 0.01$). Re-expression of WT *EB2* or *Hax1*, but not their corresponding mutants, leads to a significant increase in migration speed compared with the knockdown cells ($p < 0.01$).

Both EB2 and Hax1 Are Essential for Skin Wound Repair in Vivo—Our *in vitro* analysis clearly demonstrated the critical role of EB2/Hax1 interaction in cell adhesion dynamics and cell movement. However, the *in vivo* relevance remains unclear. Although *in vitro* approaches to explore signaling cascades controlling cell migration are readily available, the development of corresponding animal models to determine their significance *in vivo* can be costly and time-consuming. In this regard, skin epidermis provides a unique platform to investigate cell migration *in vivo* (12, 25, 26). Primary skin epidermal stem cells can be grafted to nude mice via chamber grafting (28), allowing us to examine the role of EB2/Hax1 interaction *in vivo* in a rapid and cost-effective manner. Transplantation of skin epidermal cells to nude host led to efficient skin engraftments that are stable and could readily express exogenous genes that were transduced to keratinocytes (Fig. 7, *A* and *B*).

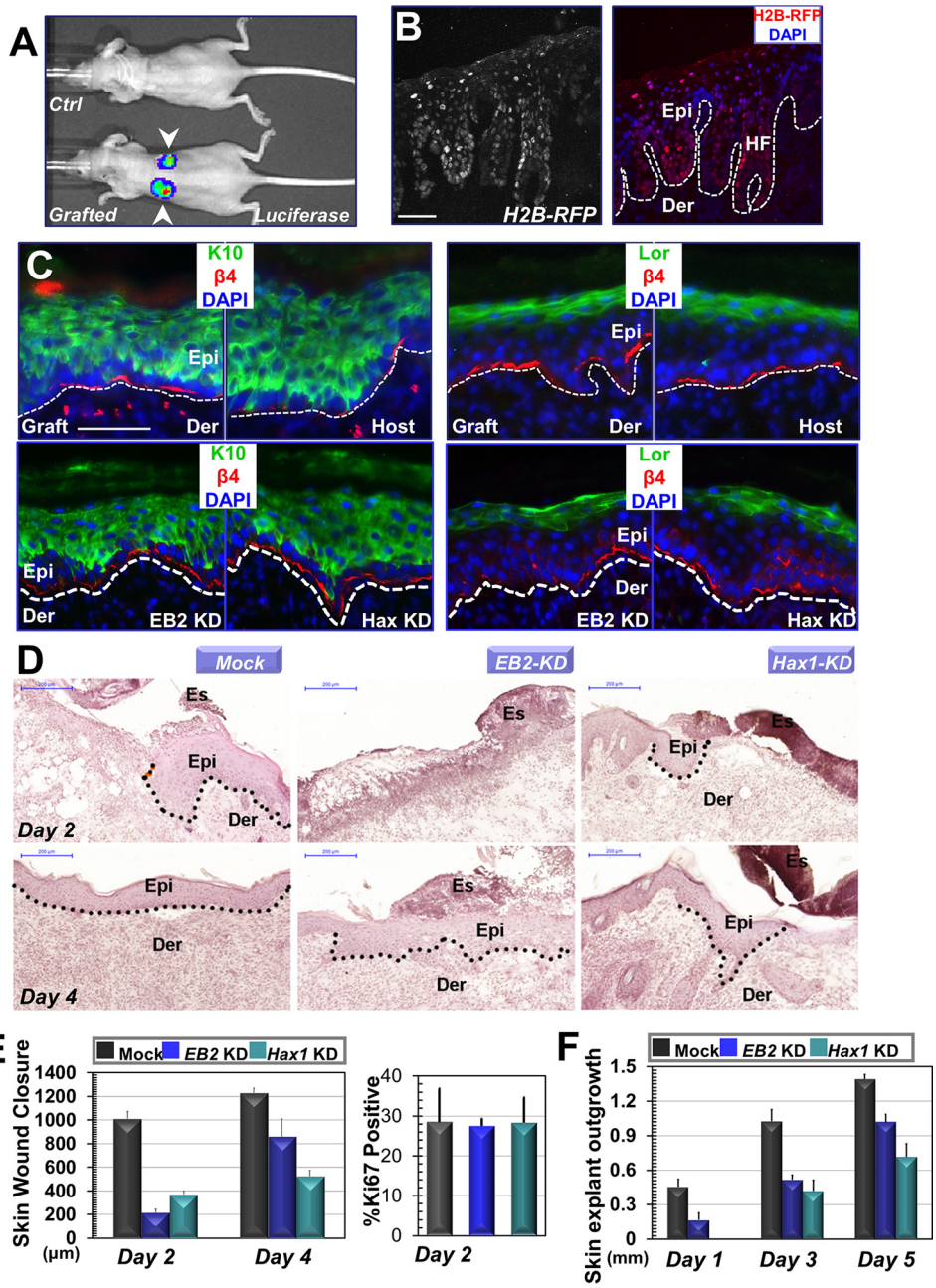

FIGURE 7. **Interaction between EB2 and Hax1 plays an essential role in skin wound healing *in vivo*.** *A*, image of nude mouse grafted with an organotypic skin culture. *Arrowheads* denote grafted skin. Intravital imaging shows efficient incorporation of grafted cells expressing luciferase upon engraftment. *Ctrl*, control. *B*, sections of nude skin with grafted H2B-RFP-expressing keratinocytes (mock, EB2 knockdown, or Hax1 knockdown) were stained with DAPI. *Dotted lines* denote dermal-epidermal boundaries. *Scale bar* = 50 μm. *Epi*, epidermis; *Der*, dermis; *HF*, hair follicle. *C*, sections of grafted skin and adjacent host skin were immunostained with different antibodies as indicated. *Dotted lines* denote dermal-epidermal boundaries. *Scale bar* = 50 μm. *K10*, keratin 10; *Lor*, Loricrin; *β4*, β4-integrin; *KD*, knockdown. *D*, wound healing as monitored by histological staining of skin sections at the wound edges 2–4 days after injury. Halves of wound sections are shown. *Dotted lines* denote dermal-epidermal boundaries. *Scale bars* = 200 μm. *Es*, eschar. *E*, *left panel*, quantification of the length of hyperproliferative epidermis generated at the indicated times after wounding ($n = 5$). *Error bars* represent mean ± S.D. Statistical analysis with Student's *t* test showed that knockdown of EB2 or Hax1 leads to a significant inhibition of wound healing at both time points compared with the mock graft ($p < 0.01$). *Right panel*, cell proliferation 2 days post-wounding was examined by Ki67 staining. Statistical analysis with Student's *t* test showed that knockdown of EB2 or Hax1 does not significantly affect cell proliferation compared with the mock sample ($n = 3, p > 0.1$). *F*, quantification of epidermal outgrowth in skin explants ($n = 3$). *Error bars* represents mean ± S.D. Statistical analysis with Student's *t* test showed that knockdown of EB2 or Hax1 leads to a significant inhibition of outgrowth at both time points compared with the mock skin explant ($p < 0.01$).

The grafted skin displayed a stratification and differentiation program indistinguishable from that of the host skin (Fig. 7*C*).

To determine the role of EB2 and Hax1 in skin wound repair, we engrafted mock keratinocytes, *EB2* knockdown cells, or *Hax1* knockdown cells to nude mice. These cells were incorporated into the host skin with comparable efficiency, and no significant difference was identified in cell proliferation or differentiation *in vivo* (Fig. 7, *C* and *E*). When grafted skins were challenged to respond to injury, both EB2 and Hax1 knockdown skins exhibited a significant delay in repairing full-thickness wounds compared with mock skin (Fig. 7, *D* and *E*). Histological analysis and quantification revealed that the area of

hyperproliferative epithelium that typically proliferates and migrates into the wound site was diminished by more than 50% on day 2 or 4 following injury in skin grafted with EB2 or Hax1 knockdown cells (Fig. 7*E*). Despite delayed wound healing, Ki67 staining results showed that there was no significant difference in cell proliferation in EB2 or Hax1 knockdown skin (Fig. 7*E*), suggesting that the wound healing defect is more likely to be rooted in aberrant cell migration.

To further explore the role of EB2 and Hax1 in skin re-epithelialization, we performed tissue explants *ex vivo* (30). The biopsies of skin grafts were placed on fibronectin-coated glass dishes and monitored for the outgrowth of interconnected epithelial sheets of grafted keratinocytes from these explants (Fig. 7*F*). Quantification revealed a marked delay in the outgrowth from *EB2* or *Hax1* knockdown explants compared with WT counterparts. Taken together, our studies present strong evidence that both EB2 and Hax1 play a critical role in epidermal migration during skin wound repair *in vivo*.

Discussion

The coordination of F-actin and microtubule dynamics is essential for a variety of cellular processes, including cell movement (2). It has been well established that focal adhesions can serve as a "hot spot" to mediate the cross-talk between microtubule and F-actin cytoskeletal networks. In mammalian cells, microtubules can specifically grow toward focal adhesions, a process likely guided by underlying F-actin filaments (8, 31). Interestingly, targeting of focal adhesions by microtubules usually leads to disassembly of focal adhesions, a feature in line with the long-standing observation that cells treated with microtubule depolymerizing drugs contain enlarged and stabilized focal adhesions (12, 32, 33). Our previous study has identified a microtubule and F-actin cross-linking protein, ACF7, as a key molecule that coordinates this process and promotes focal adhesion dynamics during cell migration (12). Our recent work has further identified MAP4K4 as a microtubule-dependent factor that can be delivered toward focal adhesion and promote focal adhesion turnover through its interaction and activation of the IQSEC1/Arf6 pathway (13). In this study, we demonstrated another critical interaction between EB2 and Hax1 that is involved in focal adhesion dynamics and cell motility. Our results indicate that depletion of endogenous EB2 or Hax1 or disruption of their interaction *in vitro* can inhibit focal adhesion turnover and diminish cell migration. By taking advantage of the skin epidermal system, we further provide evidence that EB2 and Hax1 are essential for skin wound repair and epidermal migration *in vivo*.

Growing microtubules accumulate at their plus ends multiple structurally unrelated molecules collectively termed microtubule plus end tracking proteins (14, 15). The most conserved and ubiquitous plus end proteins of microtubules are end binding proteins. Mammalian cells express three EB proteins, EB1, EB2, and EB3, that share substantial sequence similarity and can all track the plus ends of growing microtubules. Among the three proteins, EB1 is usually considered the master regulator of microtubule end dynamics because depletion of endogenous EB1 in various cell types has profound effects on microtubule organization and dynamics (16, 17). However, the role of other EB proteins, particularly EB2, remains largely unclear. It has been reported that EB1 and EB3 together can control microtubule dynamics by promoting growth and suppressing a catastrophe of microtubules, whereas EB2 is dispensable. Our recent study has unraveled a specific and essential role of EB2 in mediating the cross-talk between microtubules and focal adhesions (13). Inactivation of EB2 in cultured keratinocytes leads to aberrant focal adhesion dynamics and decreased motility, at least in part through its specific interaction with MAP4K4. On the basis of these results, we posited that EB2 might not be directly involved in the regulation of microtubule dynamic instability. Instead, via its unique sequence, EB2 may function as a plus end adaptor molecule, transforming microtubule growing ends to a dynamic signaling hot spot required for various cellular processes, including cell motility. Quantitative proteomic analysis of the EB2 interactome in this study lends further support to this hypothesis. Interestingly, unlike EB1 or EB3, our results show that EB2 associates with a diverse array of proteins, including cytoskeletal proteins, cell cycle regulators, molecules involved in membrane trafficking, and other potential signaling molecules (supplemental Tables 1–3). Although this work focuses on the interaction between EB2 and Hax1, our results revealed the complexity of the EB2 interactome, allowing us to probe deeper into the cellular function of EB2 in the future. To increase the specificity of our proteomic search, we used very stringent washing conditions during affinity purification. Therefore, although our MS analysis identified kinesin and dynactin as EB-interacting proteins, some other proteins known to associate with EB molecules were not identified, potentially because of a weaker binding affinity (supplemental Tables 1–3).

HAX1 has been shown to regulate cell migration in different systems (22–24). Depletion of endogenous Hax1 with siRNA inhibits $\alpha v\beta 6$ integrin-mediated migration of squamous cell carcinoma cells. Knockdown of Hax1 also impairs migration of NIH3T3 cells *in vitro*. Hax1 is also essential for efficient neutrophil chemotaxis and motility by regulating the detachment of uropod, integrin-mediated cell adhesion in neutrophils. In this study, we provided compelling evidence that Hax1 regulates the keratinocyte migration modulation of RhoA activity (24). Further studies will be required to decipher the molecular mechanisms whereby Hax1 regulates cell adhesion and incorporates EB2/Hax1 interaction into the signaling network controlling directional cell movement.

In closing, our findings provide critical insights into the long-standing question regarding the unique cellular function of EB2. Our results unravel a novel interaction between EB2 and Hax1 and demonstrate its relevance in focal adhesion dynamics and skin epidermal migration, paving the way for probing more deeply into the intricate signaling network underlying coordinated cytoskeletal dynamics and cell migration.

Author Contributions—X. W. conceived and coordinated the study and wrote the paper. H. L., J. Y., and X. W. designed, performed, and analyzed the experiments shown in Figs. 1–5. H. H., X. G., S. Y. C., and Y. Z. provided technical assistance and contributed to the preparation of the figures. All authors reviewed the results and approved the final version of the manuscript.

Acknowledgments—We thank Dr. Elaine Fuchs (Rockefeller University) and Dr. Jerrold Turner (University of Chicago) for sharing reagents. We thank Dr. Don Wolfgeher (University of Chicago Proteomics Core laboratory), Dr. Vytas Bindokas (University of Chicago Light Microscopy Core), and Dr. Lara Leoni (University of Chicago Animal Imaging Facilities) for technical assistance. The animal studies were carried out in the AALAC (American Association for Laboratory Animal Care)-accredited animal research facility at the University of Chicago.

References

1. Lauffenburger, D. A., and Horwitz, A. F. (1996) Cell migration: a physically integrated molecular process. *Cell* **84,** 359–369
2. Rodriguez, O. C., Schaefer, A. W., Mandato, C. A., Forscher, P., Bement, W. M., and Waterman-Storer, C. M. (2003) Conserved microtubule-actin interactions in cell movement and morphogenesis. *Nat. Cell Biol.* **5,** 599–609
3. Berrier, A. L., and Yamada, K. M. (2007) Cell-matrix adhesion. *J. Cell. Physiol.* **213,** 565–573
4. Burridge, K., and Chrzanowska-Wodnicka, M. (1996) Focal adhesions, contractility, and signaling. *Annu. Rev. Cell Dev. Biol.* **12,** 463–518
5. Delon, I., and Brown, N. H. (2007) Integrins and the actin cytoskeleton. *Curr. Opin. Cell Biol.* **19,** 43–50
6. Ridley, A. J., Schwartz, M. A., Burridge, K., Firtel, R. A., Ginsberg, M. H., Borisy, G., Parsons, J. T., and Horwitz, A. R. (2003) Cell migration: integrating signals from front to back. *Science* **302,** 1704–1709
7. Alexandrova, A. Y., Dugina, V. B., Ivanova, O. Y., Kaverina, I. N., and Vasiliev, J. M. (1998) Scatter factor induces segregation of multinuclear cells into several discrete motile domains. *Cell Motil. Cytoskeleton* **39,** 147–158
8. Kaverina, I., Krylyshkina, O., and Small, J. V. (1999) Microtubule targeting of substrate contacts promotes their relaxation and dissociation. *J. Cell Biol.* **146,** 1033–1044
9. Kaverina, I., Krylyshkina, O., Beningo, K., Anderson, K., Wang, Y. L., and Small, J. V. (2002) Tensile stress stimulates microtubule outgrowth in living cells. *J. Cell Sci.* **115,** 2283–2291
10. Krylyshkina, O., Anderson, K. I., Kaverina, I., Upmann, I., Manstein, D. J., Small, J. V., and Toomre, D. K. (2003) Nanometer targeting of microtubules to focal adhesions. *J. Cell Biol.* **161,** 853–859
11. Kodama, A., Karakesisoglou, I., Wong, E., Vaezi, A., and Fuchs, E. (2003) ACF7: an essential integrator of microtubule dynamics. *Cell* **115,** 343–354
12. Wu, X., Kodama, A., and Fuchs, E. (2008) ACF7 regulates cytoskeletal-focal adhesion dynamics and migration and has ATPase activity. *Cell* **135,** 137–148
13. Yue, J., Xie, M., Gou, X., Lee, P., Schneider, M. D., and Wu, X. (2014) Microtubules regulate focal adhesion dynamics through MAP4K4. *Dev. Cell* **31,** 572–585
14. Howard, J., and Hyman, A. A. (2003) Dynamics and mechanics of the microtubule plus end. *Nature* **422,** 753–758
15. Howard, J., and Hyman, A. A. (2009) Growth, fluctuation and switching at microtubule plus ends. *Nat. Rev. Mol. Cell Biol.* **10,** 569–574
16. Komarova, Y., De Groot, C. O., Grigoriev, I., Gouveia, S. M., Munteanu, E. L., Schober, J. M., Honnappa, S., Buey, R. M., Hoogenraad, C. C., Dogterom, M., Borisy, G. G., Steinmetz, M. O., and Akhmanova, A. (2009) Mammalian end binding proteins control persistent microtubule growth. *J. Cell Biol.* **184,** 691–706
17. Komarova, Y., Lansbergen, G., Galjart, N., Grosveld, F., Borisy, G. G., and Akhmanova, A. (2005) EB1 and EB3 control CLIP dissociation from the ends of growing microtubules. *Mol. Biol. Cell* **16,** 5334–5345
18. Kuo, J. C., Han, X., Hsiao, C. T., Yates, J. R., 3rd, and Waterman, C. M. (2011) Analysis of the myosin-II-responsive focal adhesion proteome reveals a role for β-Pix in negative regulation of focal adhesion maturation. *Nat. Cell Biol.* **13,** 383–393
19. Ong, S. E., Foster, L. J., and Mann, M. (2003) Mass spectrometric-based approaches in quantitative proteomics. *Methods* **29,** 124–130
20. Suzuki, Y., Demoliere, C., Kitamura, D., Takeshita, H., Deuschle, U., and Watanabe, T. (1997) HAX-1, a novel intracellular protein, localized on mitochondria, directly associates with HS1, a substrate of Src family tyrosine kinases. *J. Immunol.* **158,** 2736–2744
21. Klein, C., Grudzien, M., Appaswamy, G., Germeshausen, M., Sandrock, I., Schäffer, A. A., Rathinam, C., Boztug, K., Schwinzer, B., Rezaei, N., Bohn, G., Melin, M., Carlsson, G., Fadeel, B., Dahl, N., Palmblad, J., Henter, J. I., Zeidler, C., Grimbacher, B., and Welte, K. (2007) HAX1 deficiency causes autosomal recessive severe congenital neutropenia (Kostmann disease). *Nat. Genet.* **39,** 86–92
22. Radhika, V., Onesime, D., Ha, J. H., and Dhanasekaran, N. (2004) $G\alpha_{13}$ stimulates cell migration through cortactin-interacting protein Hax-1. *J. Biol. Chem.* **279,** 49406–49413
23. Ramsay, A. G., Keppler, M. D., Jazayeri, M., Thomas, G. J., Parsons, M., Violette, S., Weinreb, P., Hart, I. R., and Marshall, J. F. (2007) HS1-associated protein X-1 regulates carcinoma cell migration and invasion via clathrin-mediated endocytosis of integrin αvβ6. *Cancer Res.* **67,** 5275–5284
24. Cavnar, P. J., Berthier, E., Beebe, D. J., and Huttenlocher, A. (2011) Hax1 regulates neutrophil adhesion and motility through RhoA. *J. Cell Biol.* **193,** 465–473
25. Blanpain, C., and Fuchs, E. (2006) Epidermal stem cells of the skin. *Annu. Rev. Cell Dev. Biol.* **22,** 339–373
26. Wu, X., Shen, Q. T., Oristian, D. S., Lu, C. P., Zheng, Q., Wang, H. W., and Fuchs, E. (2011) Skin stem cells orchestrate directional migration by regulating microtubule-ACF7 connections through GSK3β. *Cell* **144,** 341–352
27. Schober, M., Raghavan, S., Nikolova, M., Polak, L., Pasolli, H. A., Beggs, H. E., Reichardt, L. F., and Fuchs, E. (2007) Focal adhesion kinase modulates tension signaling to control actin and focal adhesion dynamics. *J. Cell Biol.* **176,** 667–680
28. Guasch, G., Schober, M., Pasolli, H. A., Conn, E. B., Polak, L., and Fuchs, E. (2007) Loss of TGFβ signaling destabilizes homeostasis and promotes squamous cell carcinomas in stratified epithelia. *Cancer Cell* **12,** 313–327
29. Dixit, R., and Ross, J. L. (2010) Studying plus-end tracking at single molecule resolution using TIRF microscopy. *Methods Cell Biol.* **95,** 543–554
30. Mazzalupo, S., Wawersik, M. J., and Coulombe, P. A. (2002) An *ex vivo* assay to assess the potential of skin keratinocytes for wound epithelialization. *J. Invest. Dermatol.* **118,** 866–870
31. Krylyshkina, O., Kaverina, I., Kranewitter, W., Steffen, W., Alonso, M. C., Cross, R. A., and Small, J. V. (2002) Modulation of substrate adhesion dynamics via microtubule targeting requires kinesin-1. *J. Cell Biol.* **156,** 349–359
32. Bershadsky, A., Chausovsky, A., Becker, E., Lyubimova, A., and Geiger, B. (1996) Involvement of microtubules in the control of adhesion-dependent signal transduction. *Curr. Biol.* **6,** 1279–1289
33. Ezratty, E. J., Partridge, M. A., and Gundersen, G. G. (2005) Microtubule-induced focal adhesion disassembly is mediated by dynamin and focal adhesion kinase. *Nat. Cell Biol.* **7,** 581–590